



# Direct Coupling Strategy in Plasmonic Nanocircuits for Low Loss and Easy Fabrication

Zhaojian Zhang<sup>1</sup> · Junbo Yang<sup>2</sup> · Yunxin Han<sup>2</sup> · Xin He<sup>2</sup> · Jie Huang<sup>1</sup> · Dingbo Chen<sup>1</sup>

Received: 29 August 2019 / Accepted: 4 December 2019 / Published online: 11 December 2019  
© Springer Science+Business Media, LLC, part of Springer Nature 2019

## Abstract

Plasmonic nanocircuits can deliver light in subwavelength scale, however, require state-of-the-art fabrication process due to the ultra-small footprints. Here, we introduce direct coupling strategy based on metal-insulator-metal (MIM) waveguide systems to reduce the system loss as well as the fabrication difficulty and increase the structural stability. Following this strategy, the coupling between the input waveguide and square ring resonator (SRR) can be realized via an aperture, and for the coupling between SRRs, the metal gap can be removed. The numerical results show that such direct coupling can produce similar effects with conventional indirect coupling in MIM waveguide systems, and the physics mechanism behind as well as influences of geometric parameters on transmission spectrum is also investigated. This work provides a simpler approach to realize on-chip plasmonic nanodevices, such as filters, sensors, and optical delay lines, in practice.

**Keywords** Metal-insulator-metal · Direct coupling · Easy fabrication

## Introduction

Surface plasmon polaritons (SPPs), which are electromagnetic waves existing on the interface between dielectrics and metals, have been playing an important role in modern nanophotonics [1]. SPPs have the capacity to break the diffraction limit, therefore can support and deliver light in subwavelength scale [2]. Up to now, SPPs have brought plasmonic nano-systems such as metasurfaces [3] and nanophotonic circuits [4], paving the way to the realization of novel photonic nanodevices such as label-free sensors [5–7], high-speed modulators [8–10], and nanolasers [11–13]. Especially, compared with conventional dielectric circuits, plasmonic nanocircuits have much smaller footprints, therefore can meet the requirement of on-chip highly integrated photonic circuits [14].

Among all kinds of plasmonic nanocircuits, metal-insulator-metal (MIM) waveguide systems have drawn more attention due to the deep subwavelength confinement, considerable propagation length, and easy fabrication [15]. Various

MIM waveguide devices, such as filters, spacers, and logic gates, have been realized experimentally [16–20] and numerically [21–25]. To build such systems, waveguides as well as resonators are directly etched on thin metal films, and the coupling arrangements between waveguides and resonators are similar with those in dielectric photonic circuits, such as silicon circuits [26]. However, the coupling areas between the two components, which are air in silicon circuits, turn into metal gaps in MIM waveguide systems as shown in Fig. 1 a and c, and the coupling distances are usually between 10 and 20 nm. Obviously, such indirect coupling strategy will bring about more ohmic loss induced by metals. What's more, it has been reported that thicker MIM waveguides possess lower propagation loss, and the thickness must be more than 100 nm to get an acceptable loss in the infrared [27]. In such case, the gap will become a thin metal wall as indicated in Fig. 1 a and c, which requires state-of-the-art fabrication process and is also prone to collapse after fabrication.

In this paper, we introduce direct coupling strategy based on square ring resonators (SRRs) as given in Fig. 1 b and d. For the coupling between the waveguide and resonator, an aperture is utilized for the direct connection. As for the coupling between resonators, the metal gap is removed. Our numerical results show that direct coupling can produce similar effects with conventional indirect coupling in MIM coupling systems, and the physics mechanism behind as well as influences of geometric parameters on transmission spectrum is

✉ Zhaojian Zhang  
376824388@qq.com

<sup>1</sup> College of Liberal Arts and Sciences, National University of Defense Technology, Changsha 410073, China

<sup>2</sup> Center of Material Science, National University of Defense Technology, Changsha 410073, China

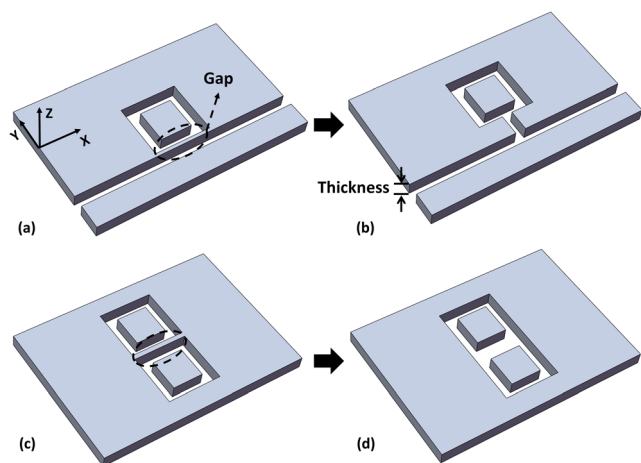


**Fig. 1** **a** The indirect coupling between the waveguide and resonator in a MIM system. **b** The direct coupling between the waveguide and resonator in a MIM system. **c** The indirect coupling between the two resonators in a MIM system. **d** The direct coupling between the two resonators in a MIM system

also investigated. This work provides a strategy to build MIM waveguide nanocircuits with easier fabrication, better structural stability, and less loss. This work is valuable for realizing

ultracompact plasmonic nanodevices in practice such as filters, sensors, and optical delay lines.

### Structures and Methods

The two-dimensional (2D) scheme of proposed structure is shown in Fig. 2 a, including an input waveguide and an aperture-coupled SRR. The geometric parameters are as follows:  $w = 50$  nm,  $d = 600$  nm,  $h = 130$  nm,  $L = 385$  nm. The white area is air and gray area is silver (Ag). The permittivity of Ag is described by Drude model [28]:

$$\epsilon_m = \epsilon_\infty - \frac{\omega_p^2}{\omega(\omega + i\gamma)} \tag{1}$$

where  $\epsilon_m$  is the permittivity of Ag,  $\epsilon_\infty$  is the permittivity at infinite frequency,  $\omega_p$  is the bulk plasma frequency,  $\gamma$  is the electron oscillation damping frequency, and  $\omega$  is the angular frequencies of incident waves. The parameters of Ag are as follows:  $\epsilon_\infty = 3.7$ ,  $\omega_p = 1.38 \times 10^{16}$  Hz, and  $\gamma = 2.73 \times 10^{13}$  Hz.

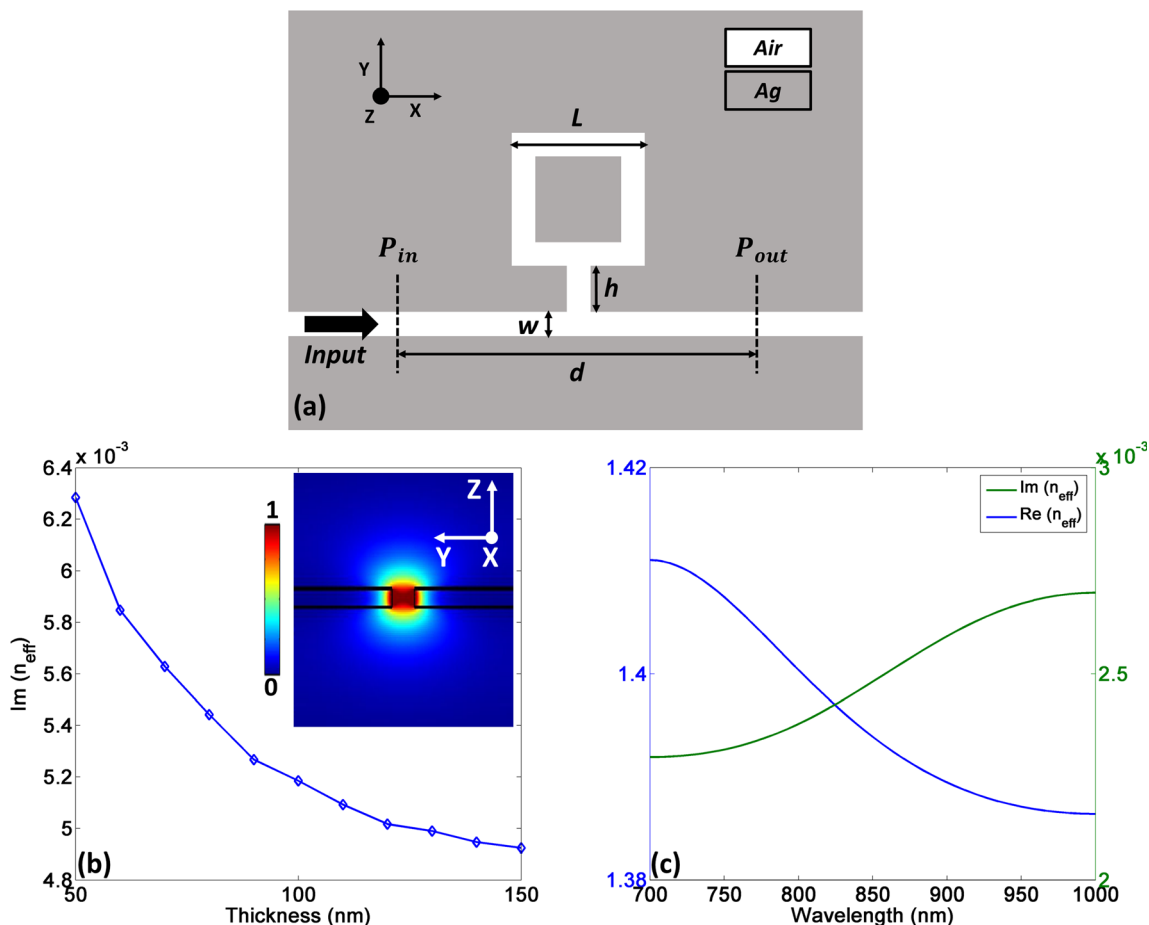


**Fig. 2** **a** The 2D scheme of proposed structure and the geometric parameters are as follows:  $w = 50$  nm,  $d = 600$  nm,  $h = 130$  nm,  $L = 385$  nm. **b** The relation between imaginary parts of fundamental mode

and the thickness at 700 nm. The inset is the mode distribution  $H_z$  on the cross section of the waveguide. **c** The calculated  $n_{eff}$  of fundamental TM mode in 2D case from 700 to 1000 nm

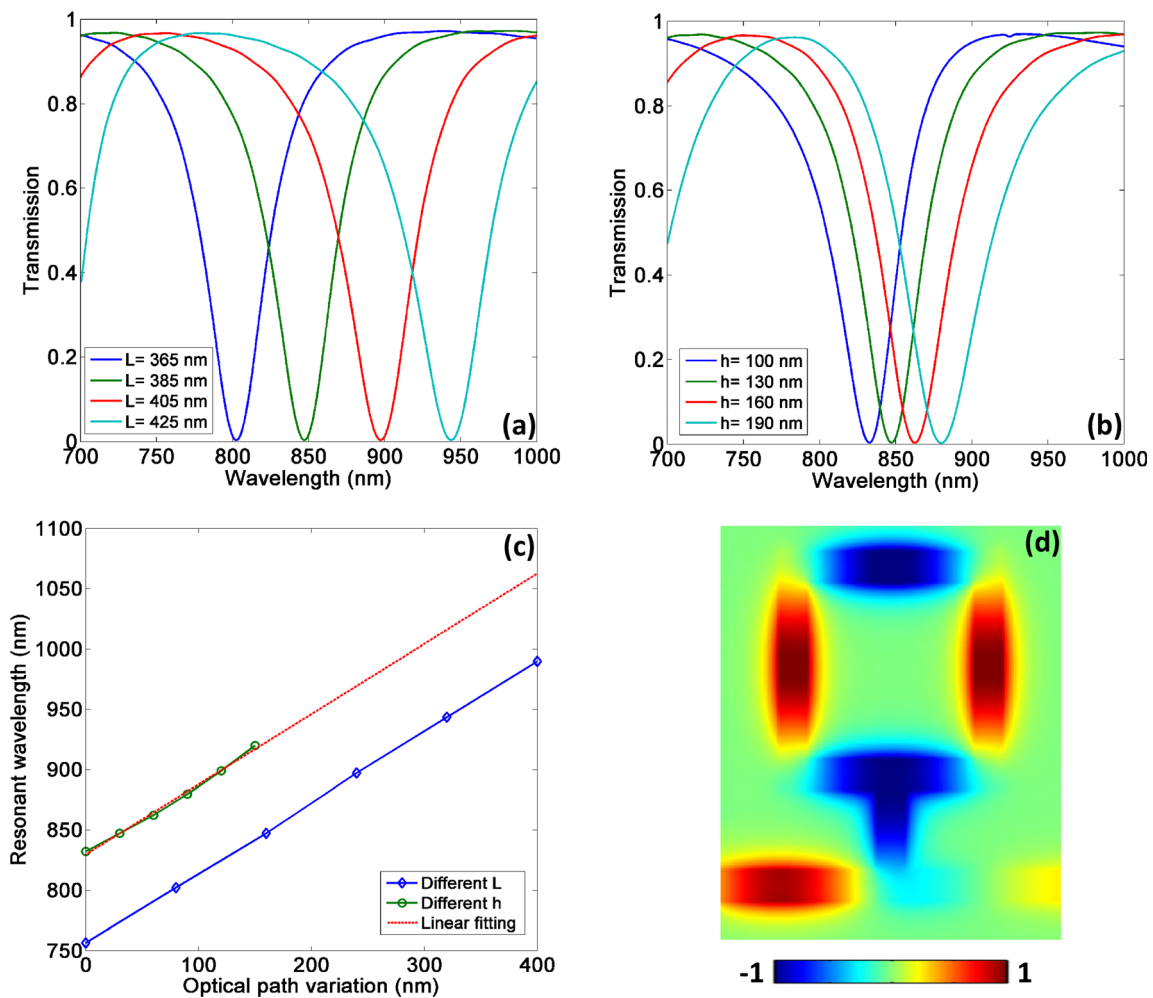


**Fig. 3** **a** The transmission spectrum under different side length  $L$  of SRR. **b** The transmission spectrum under different aperture lengths  $h$ . **c** The relation between resonant wavelengths and optical path variation. **d** The mode  $H_z$  distribution at 847 nm when  $L = 385$  nm and  $h = 130$  nm

MIM waveguides can only support transverse-magnetic (TM) SPP mode, and since the width  $w$  of the waveguide is much smaller than the input wavelength, there is only fundamental TM mode [29]. The dispersion relation of the fundamental mode is described as follows [30]:

$$\frac{\epsilon_i \sqrt{\beta^2 - \epsilon_m k_0^2}}{\epsilon_m \sqrt{\beta^2 - \epsilon_i k_0^2}} + \tanh\left(\frac{w \sqrt{\beta^2 - \epsilon_i k_0^2}}{2}\right) = 0 \quad (2)$$

where  $\epsilon_i$  is the permittivity of the insulator,  $k_0 = 2\pi/\lambda_0$  is the wave vector in free space, and  $\beta$  is the wave vector of SPPs in MIM waveguides. The effective refractive index is defined as  $n_{eff} = \beta/k_0$ . It is known that wider MIM waveguides will possess lower propagation loss [27]. Considering the balance between loss and footprint, the width of the waveguide is kept as 50 nm [15].

Lumerical 2D finite-difference time-domain (FDTD) solution, which considers the size in the third dimension (the thickness of the metal film) as infinite, is used to do the

simulation, and it has to be mentioned that such method is utilized mostly in MIM waveguide works since it can save the computational memory [15, 21–25, 31, 32], and it has been reported that 3D simulation will have same results as

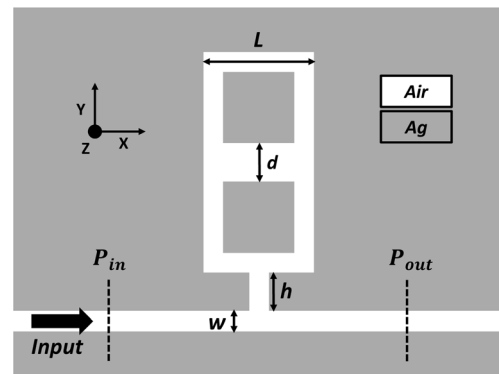


**Fig. 4** The proposed direct coupling structure with two resonators, and the geometric parameters are as follows:  $w = 50$  nm,  $h = 130$  nm,  $L = 385$  nm, and coupling distance  $d = 100$  nm

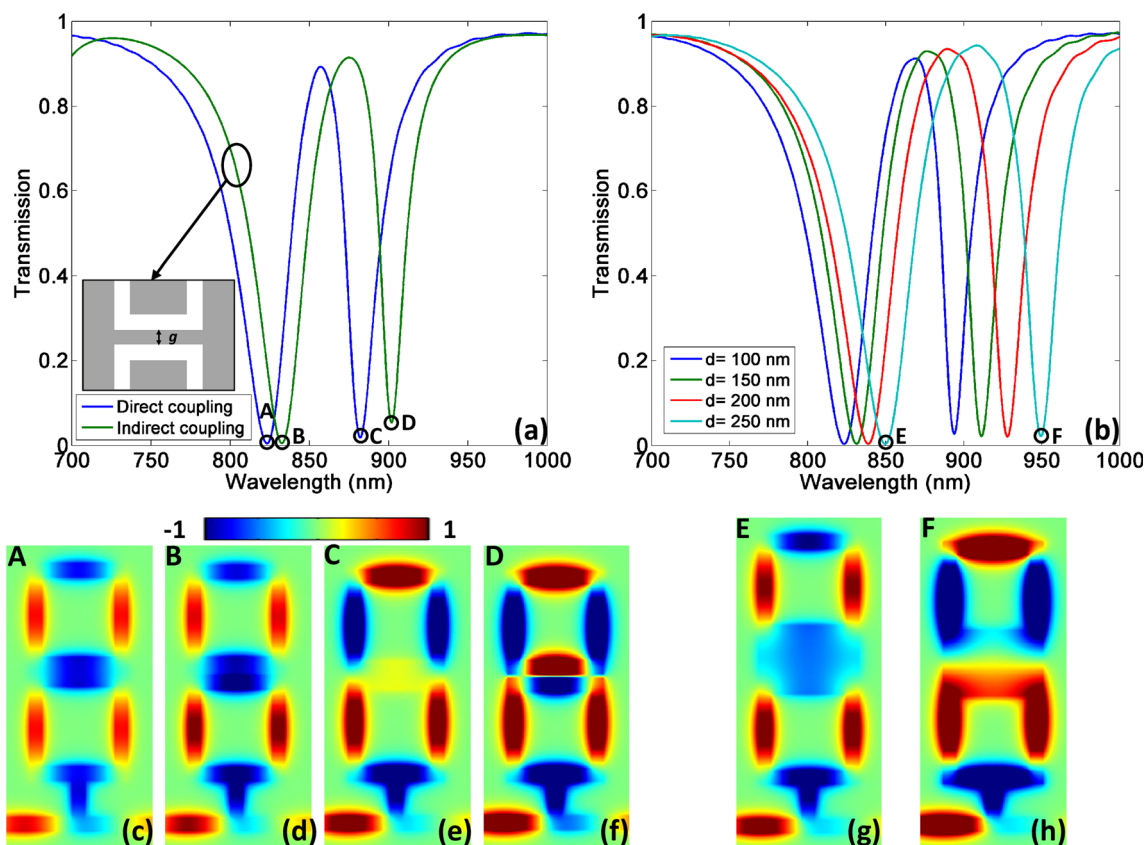


**Fig. 5** **a** The transmission spectrum of direct coupling and indirect coupling structure. The inset shows the metal gap of indirect coupling structure with  $g = 15$  nm, and the other geometrical parameters are same

as Fig. 4. **b** The transmission spectrum of direct coupling structure with different coupling distance  $d$ . **c–f** The mode distributions at position A, B, C, and D in **a**. **g–h** The mode distributions at position E and F in **b**

2D simulation when the thickness reaches  $1 \mu\text{m}$  [33, 34]. Here, we also simulate the 3D MIM waveguide with width 50 nm to study the relation between the propagation loss and the thickness of the waveguide. The imaginary parts, which represent the loss, of the fundamental TM mode under different thicknesses at 700 nm are shown in Fig. 2 b, and the mode distribution ( $Z$  component of magnetic field  $H_z$ ) on the cross section of the waveguide is given in the inset of Fig. 2 b. Obviously, the loss decreases when increasing the thickness from 50 to 150 nm, which confirms that thicker waveguides will possess lower propagation loss. The calculated  $n_{\text{eff}}$  of fundamental TM mode in 2D case from 700 to 1000 nm are also shown in Fig. 2 c. In the simulation domain, the mesh size is chosen as 3 nm to ensure the accuracy, and the absorbing boundary conditions are set as perfectly matched layers (PMLs) at all boundaries to maintain convergence. Two power monitors are arranged at  $P_{\text{in}}$  and  $P_{\text{out}}$ , respectively, and the transmission is calculated as  $T = P_{\text{out}}/P_{\text{in}}$ .

### Results and Discussion

The transmission spectrum of the aperture-coupled SRR in Fig. 2 a under different side lengths  $L$  of SRR are shown in

Fig. 3 a; the aperture length  $h$  is kept as 130 nm. The Lorentz line shapes of the spectrum indicate that there is a resonant mode in SRR, and increasing  $L$  will lead to red shifts in the spectrum. The results are similar when increasing  $h$  while  $L$  is kept as 385 nm, as given in Fig. 3 b. Figure 3 c provides the relation between resonant wavelengths and optical path variation, where the variation is defined as length changes of  $L$  or

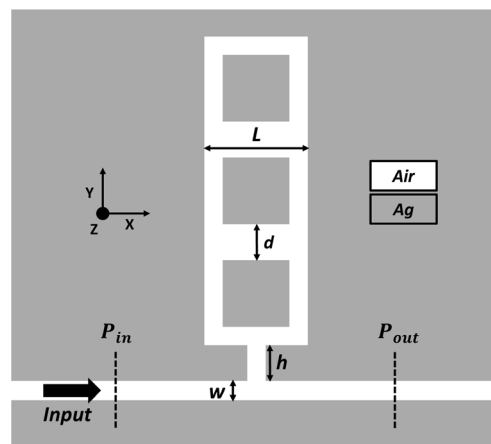


**Fig. 6** The proposed direct coupling structure with multiple resonators. The geometric parameters are as follows:  $w = 50$  nm,  $h = 130$  nm,  $L = 385$  nm, and each coupling distance  $d$  is 100 nm

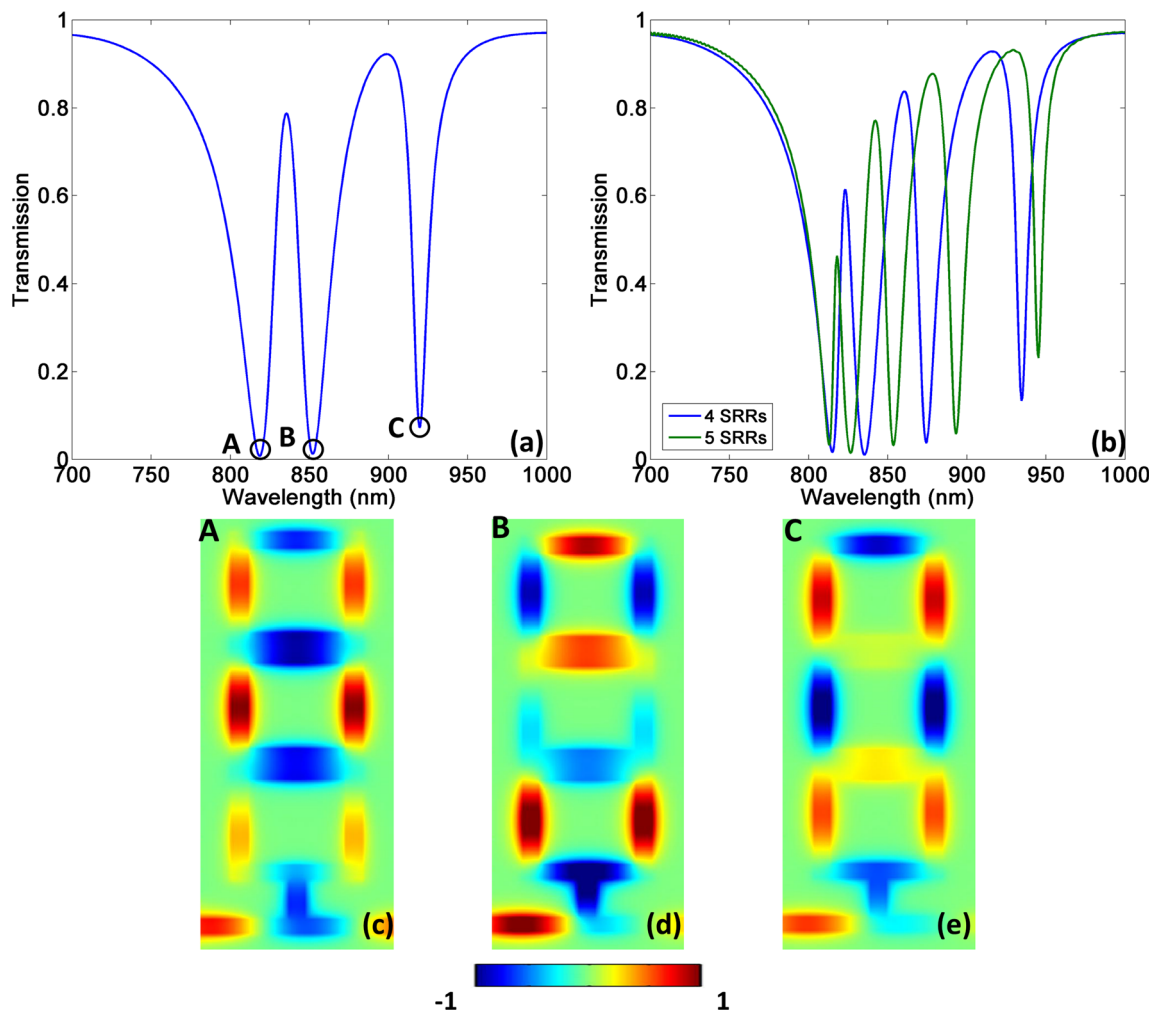


**Fig. 7** **a** The transmission spectrum of proposed direct coupling structure with three SRRs. **b** The transmission spectrum of proposed direct coupling structure with four and five SRRs. **c–e** The mode distributions at position A, B, and C in **a**

$h$ , and from which we can see that resonant wavelengths have linear relations with both variations of  $L$  and  $h$ , and the two variations contribute equally to the shift of resonant wavelengths. We also investigate the mode  $H_z$  distribution at 847 nm when  $L = 385$  nm and  $h = 130$  nm, as shown in Fig. 3 d. The mode profile indicates that it is a typical ring traveling-wave mode (TWM) and the resonant condition can be expressed as follows:

$$n\lambda = (4L_{eff} + h_{eff})\text{Re}(n_{eff}), n = 1, 2, 3... \quad (3)$$

where  $L_{eff}$  and  $h_{eff}$  are the effective side length of SRR and length of aperture, respectively, which can be estimated from the mode distribution.  $n$  is the mode order number, which is an integer. For instance, when  $L = 385$  nm and  $h = 130$  nm, the resonant wavelength is 847 nm, and  $\text{Re}(n_{eff})$  is 1.394 as given in Fig. 2 c. From Fig. 3 d, we can see that there is no field distribution at the four corners of SRR; therefore,  $L_{eff}$  is 285 nm. The aperture is filled with magnetic field so  $h_{eff} = 130$  nm. Consequently, we can get  $n = 2$  approximately

following Eq. (3), which accords with the mode order indicated in Fig. 3 d.

The proposed direct coupling strategy between two resonators is shown in Fig. 4. Compared with indirect coupling strategy, the metal gap is removed, the coupling distance  $d$  between two SRRs is set as 100 nm, and the corresponding transmission spectrum is given in Fig. 5 a. For comparison, we also depict the transmission spectrum of the structure with gap in Fig. 5 a, the structure is described in the inset of Fig. 5 a, and the coupling distance, i.e., the metal gap width  $g$ , is 15 nm. It is shown that both coupling strategies possess two transmission dips, which indicate two resonances. The mode distributions at each dip are presented in Fig. 5 c–f. For conventional indirect coupling strategy, the coupling will introduce a frequency splitting, which can be described by two supermodes at position B and D, i.e., the symmetric supermode with in-phase field distributions between the two SRRs as described in Fig. 5 d, and the antisymmetric supermode with out-phase field distributions as described in Fig. 5 f [35].



For direct coupling strategy, there is also a symmetric supermode at position A. The absence of metal gap has no influence on the supermode distribution as presented in Fig. 5 c, but will change the coupling strength between the two basic modes in each SRR, which will lead to a blue shift of resonant wavelength as indicated in Fig. 5 a. The mode at position C, however, is no longer the antisymmetric supermode as shown in Fig. 5 e. Actually, the resonant light waves only propagate along the perimeter path as indicated in Fig. 5 e, and there is no field distribution in the space between the two SRRs. Therefore, it is a typical TWM. We also investigate the impact of coupling distance  $d$  on the transmission spectrum as shown in Fig. 5 b. It is shown that both transmission dips will have a red shift with the increasing coupling distance, and obviously, the right dip has a much larger shift than the left dip. The mode distributions at two dips when  $d = 250$  nm are given in Fig. 5 g and h, respectively. For the mode at left dip, Fig. 5 g shows that the larger  $d$  does not disturb the mode distribution in the edges of SRRs, the mode in each SRR still has the same in-phase distribution as Fig. 5 c. Consequently, the larger  $d$  does not change the resonant wavelength of the basic mode in each SRR, but only influences the coupling strength between the two SRRs, leading to the slight red shift of the left dip. However, the resonant wavelength of the TWM at right dip is sensitive to the length of perimeter paths, therefore possesses a more significant red shift. Such mechanism provides an approach to tune the free spectral range (FSR) between the two resonances.

Furthermore, the direct coupling of multiple resonators is also investigated as shown in Fig. 6, and each coupling distance is 100 nm. Here, three SRRs are directly cascaded, and three transmission dips appear as shown in Fig. 7 a; the mode distribution at each dip is depicted in Fig. 7 c–e. It is shown that for the mode at dip A, the magnetic field is concentrated in the two SRRs above. The field is concentrated in the top and bottom SRRs for the mode at dip B. For the mode at dip C, a typical TWM along the perimeter path is formed. If more resonators are introduced, there will be more resonant dips in the transmission spectrum. There are four transmission dips when four SRRs are directly coupled as shown by blue line in Fig. 7 b, and five dips for five SRRs as given by green line in Fig. 7 b. Therefore, such direct coupling strategy is still compatible when multiple resonators are introduced and can be applied in more complex plasmonic chip-scale systems. Such cascade structure also has potential applications in multi-spectral sensing and filtering.

At last, we will discuss about the superiority of direct coupling compared with indirect coupling. First, the ultranarrow metal gaps (normally in the scale of 10 to 20 nm) are totally absent in direct coupling strategy, which will greatly reduce the accuracy requirement of fabricating process. Consequently, such direct coupling structure only consists of waveguides with a width of dozens of nanometers and can be

easily fabricated by focused ion beam (FIB) etching system in practice [16–20]. Besides, since gaps are easy-collapsed thin metal walls in 3D case, the absence of such gaps will increase the stability of the whole structure, and the metal film therefore can thicken at will to gain an acceptable propagation loss in the waveguides. What's more, a lack of gaps will also lead to a lower intrinsic loss, which mainly attributes to the ohmic loss of metal.

## Conclusion

In summary, we propose a direct coupling strategy based on plasmonic MIM waveguide nanocircuits. Following this strategy, the proposed SRR can be directly coupled with the waveguide via an aperture, and the direct coupling between SRRs possesses no metal gap. Such strategy provides an approach to design MIM devices with easy fabrication, better structural stability as well as low loss, and can enhance the realization of various chip-scale plasmonic nanodevices in practice such as filters, sensors, and optical delay lines.

**Funding information** This work is supported by the National Natural Science Foundation of China (61671455, 61805278), the Foundation of NUDT (ZK17-03-01), the Program for New Century Excellent Talents in University (NCET-12-0142), and the China Postdoctoral Science Foundation (2018 M633704).

## References

- Ozby E (2006) Plasmonics: merging photonics and electronics at nanoscale dimensions. *Science* 311(5758):189–193
- Gramotnev DK, Bozhevolnyi SI (2010) Plasmonics beyond the diffraction limit. *Nat Photonics* 4(2):83
- Meinzer N, Barnes WL, Hooper IR (2014) Plasmonic meta-atoms and metasurfaces. *Nat Photonics* 8(12):889
- Fang Y, Sun M (2015) Nanoplasmonic waveguides: towards applications in integrated nanophotonic circuits. *Light Sci Appl* 4(6):e294
- Stewart ME, Anderton CR, Thompson LB, Maria J, Gray SK, Rogers JA, Nuzzo RG (2008) Nanostructured plasmonic sensors. *Chem Rev* 108(2):494–521
- Liu N, Mesch M, Weiss T, Hentschel M, Giessen H (2010) Infrared perfect absorber and its application as plasmonic sensor. *Nano Lett* 10(7):2342–2348
- Im H, Shao H, Park YI, Peterson VM, Castro CM, Weissleder R, Lee H (2014) Label-free detection and molecular profiling of exosomes with a nano-plasmonic sensor. *Nat Biotechnol* 32(5):490–495
- Melikyan A, Alloatti L, Muslija A, Hillerkuss D, Schindler PC, Li J et al (2014) High-speed plasmonic phase modulators. *Nat Photonics* 8(3):229
- Hössbacher C, Josten A, Baeuerle B, Fedoryshyn Y, Hettrich H, Salamin Y et al (2017) Plasmonic modulator with > 170 GHz bandwidth demonstrated at 100 GBd NRZ. *Opt Express* 25(3):1762–1768

10. Ayata M, Fedoryshyn Y, Heni W, Baeuerle B, Josten A, Zahner M et al (2017) High-speed plasmonic modulator in a single metal layer. *Science* 358(6363):630–632
11. Oulton RF, Sorger VJ, Zentgraf T, Ma RM, Gladden C, Dai L et al (2009) Plasmon lasers at deep subwavelength scale. *Nature* 461(7264):629
12. Gather MC (2012) A rocky road to plasmonic lasers. *Nat Photonics* 6(11):708
13. Sidiropoulos TP, Röder R, Geburt S, Hess O, Maier SA, Ronning C, Oulton RF (2014) Ultrafast plasmonic nanowire lasers near the surface plasmon frequency. *Nat Phys* 10(11):870
14. Bozhevolnyi SI, Volkov VS, Devaux E, Laluet JY, Ebbesen TW (2006) Channel plasmon subwavelength waveguide components including interferometers and ring resonators. *Nature* 440(7083):508–511
15. Lu H, Wang G, Liu X (2013) Manipulation of light in MIM plasmonic waveguide systems. *Chin Sci Bull* 58(30):3607–3616
16. Yang X, Hu X, Chai Z, Lu C, Yang H, Gong Q (2014) Tunable ultracompact chip-integrated multichannel filter based on plasmon-induced transparencies. *Appl Phys Lett* 104(22):221114
17. Naghizadeh S, Afridi A, Arisev O, Karasahin A, Kocabaş ŞE (2017) Experimental investigation of stub resonators built in plasmonic slot waveguides. *IEEE Photon Technol Lett* 29(8):663–666
18. Zhu Y, Hu X, Yang H, Gong Q (2014) On-chip plasmon-induced transparency based on plasmonic coupled nanocavities. *Sci Rep* 4:3752
19. Yang X, Hu X, Yang H, Gong Q (2017) Ultracompact all-optical logic gates based on nonlinear plasmonic nanocavities. *Nanophotonics* 6(1):365
20. Kriesch A, Burgos SP, Ploss D, Pfeifer H, Atwater HA, Peschel U (2013) Functional plasmonic nanocircuits with low insertion and propagation losses. *Nano Lett* 13(9):4539–4545
21. Lu H, Liu X, Gong Y, Mao D, Wang L (2011) Enhancement of transmission efficiency of nanoplasmonic wavelength demultiplexer based on channel drop filters and reflection nanocavities. *Opt Express* 19(14):12885–12890
22. Hu F, Yi H, Zhou Z (2011) Wavelength demultiplexing structure based on arrayed plasmonic slot cavities. *Opt Lett* 36(8):1500–1502
23. Fu H, Li S, Wang Y, Song G, Zhang P, Wang L, Yu L (2018) Independently tunable ultrasharp double fano resonances in coupled plasmonic resonator system. *IEEE Photonics J* 10(1):1–9
24. Zhang Z, Yang J, He X, Han Y, Zhang J, Huang J et al (2018) All-optical multi-channel switching at telecommunication wavelengths based on tunable plasmon-induced transparency. *Opt Commun* 425:196–203
25. Nozhat N, Granpayeh N (2015) All-optical logic gates based on nonlinear plasmonic ring resonators. *Appl Opt* 54(26):7944–7948
26. Almeida VR, Barrios CA, Panepucci RR, Lipson M (2004) All-optical control of light on a silicon chip. *Nature* 431(7012):1081–1084
27. Veronis G, Fan S (2007) Modes of subwavelength plasmonic slot waveguides. *J Lightwave Technol* 25(9):2511–2521
28. Johnson PB, Christy RW (1972) Optical constants of the noble metals. *Phys Rev B* 6(12):4370–4379
29. Dionne J, Sweatlock L, Atwater H, Polman A (2006) Plasmon slot waveguides: towards chip-scale propagation with subwavelength-scale localization. *Phys Rev B* 73(3)
30. Gordon R, Brolo AG (2005) Increased cut-off wavelength for a subwavelength hole in a real metal. *Opt Express* 13(6):1933–1938
31. Veronis G, Yu Z, Kocabaş SE, Miller DA, Brongersma ML, Fan S (2009) Metal-dielectric-metal plasmonic waveguide devices for manipulating light at the nanoscale. *Chin Opt Lett* 7(4):302–308
32. Naghizadeh S, Kocabaş ŞE (2017) Guidelines for designing 2D and 3D plasmonic stub resonators. *JOSA B* 34(1):207–217
33. Bahramipناه M, Abrishamian MS, Mirtaheri SA, Liu JM (2014) Ultracompact plasmonic loop–stub notch filter and sensor. *Sensors Actuators B Chem* 194:311–318
34. He Z, Li H, Li B, Chen Z, Xu H, Zheng M (2016) Theoretical analysis of ultrahigh figure of merit sensing in plasmonic waveguides with a multimode stub. *Opt Lett* 41(22):5206–5209
35. Haus HA (1984) *Waves and fields in optoelectronics* (1984). Prentice-Hall, Englewood Cliffs, NJ

**Publisher's Note** Springer Nature remains neutral with regard to jurisdictional claims in published maps and institutional affiliations.